THE STRUCTURAL DESIGN OF TALL AND SPECIAL BUILDINGS
Struct. Design Tall Spec. Build. (2009)
Published online in Wiley Interscience (www.interscience.wiley.com). **DOI**: 10.1002/tal.515

NUMERICAL STUDIES ON THE APPLICATION OF TUNED LIQUID DAMPERS WITH SCREENS TO CONTROL SEISMIC RESPONSE OF STRUCTURES

A. M. HALABIAN* AND M. TORKI
Department of Civil Engineering, Isfahan University of Technology, Isfahan, 84156-83111, Islamic Republic of Iran

SUMMARY

Tuned liquid damper (TLD) systems are nowadays increasingly being used as one of the economical and effective passive vibration absorbers. A TLD system consists of a water tank having the fundamental sloshing fluid frequency tuned to the frequency near to the natural frequency of structure. This research focuses on modelling tall buildings equipped with TLDs having inside screens subjected to strong ground motions. Strong excitation can cause wave-breaking phenomenon and makes turbulent in shallow rectangular tanks which could also contribute to the additional damping due to TLDs. On the other hand, wire screens placed inside a liquid tank can play an important role in reducing the structural response due to increasing the inherent damping of the structure. Based on equalizing dissipated energies, a TLD equipped with internal screens can be modelled by equivalent amplitude-dependent tuned mass damper (TMD). In this study, adopting this simple method, equations of motion for shear-type buildings equipped with nonlinear amplitude-dependent TMDs were developed. A complex modal analysis procedure was used to solve the governing equations. Coupling of TMD properties and structural response was solved with iteration on structural response and updating TMD properties. Performing a set of parametric studies on three proposed tall structures equipped with TLD subjected to different ground excitations showed that if the TLD is tuned to a frequency close to the natural frequency of the structure considering hardening behaviour of TLD, it could significantly reduce the seismic response (displacements and base shears) of the structures. Copyright © 2009 John Wiley & Sons, Ltd.

1. INTRODUCTION

Damping is one of the most important parameters that limit the response of structures during extreme events. Tuned liquid dampers (TLDs) are now emerging as one of new passive control devices, which increase the damping of the structure during excitation. The sloshing motion of the fluid that results from the vibration of the structure dissipates a portion of the energy released by the dynamic loading, and therefore increases the equivalent damping of the structure. However, due to the turbulent behaviour of the inside fluid during strong excitations, the TLD provides not such a very clear mechanism of damping that can be quantified in a definite manner. The design of a TLD as a control device requires reasonably accurate considering wave-breaking phenomenon followed by turbulent in shallow tanks to evaluate the amount and type of additional inherent damping due to TLD. Furthermore, wire screens placed inside a liquid tank can play an alternative way to increase the inherent damping of the structure and also to overcome the complexity of evaluating the dynamic parameters of the TLD.

*Correspondence to: Amir M. Halabian, Department of Civil Engineering, Isfahan University of Technology, Isfahan, 84156-83111, Islamic Republic of Iran. E-mail: mahdi@cc.iut.ac.ir

In the past few years, TLD systems have been used as vibration absorber in several buildings to reduce the level of vibrations of the structures during their normal operation (Wakahara *et al*., 1992). The application of this kind of absorber to flexible structures such as tall structures for the mitigation of wind-induced vibration has been investigated by many researchers (Sakai *et al*., 1991; Xu *et al*., 1992; Balendra *et al*., 1995). The applicability of this device to seismic vibration control is also a topic of current research interest. This has been explored by Haroun *et al*. (1994), Sun (1994), Won *et al*. (1996) and Yalla and Kareem (2000) among others.

As it was pointed out for TLDs, an increase in inherent damping can be achieved by attaching a number of screens inside the tank (Noji *et al*., 1988; Kaneko and Ishikawa, 1999). Noji (1990) used wire screens to maximize the damping of water sloshing and prevent wave braking in higher amplitude excitations. He installed screens at the centre of the tank in a vertical direction and could control the velocity in the horizontal direction, and showed that this arrangement for the screens leads to an increase to the dissipated energy. The vertical velocity as the factor that improves the predicted damping capacity of the sloshing fluid was considered in a research conducted by Young (2004). Placing the embossment against the end walls of the tank reduces the vertical velocity and dissipates more energy, resulting in an increase in the damping of TLD. Tait *et al*. (2004) experimentally studied the application of TLDs with internal damping screens to mitigate dynamic response of structures and developed an equivalent amplitude-dependent simple tuned mass damper (TMD) model based on the test results on a shaking table device.

The current study was aimed to examine the seismic response of TLD structure systems implementing the approach developed by Tait *et al*. (2004) where the equivalent amplitude-dependent simple TMD was introduced. The application of single or multiple TLD(s) attached to tall shear-type structures subjected to unidirectional excitations is studied. Having non-classical damping resulting from TLD (equivalent amplitude-dependent TMD), a complex modal analysis method is developed to solve the governing equations. The ratio of TLD mass to the modal mass of the structure is recognized as one of the important parameters affecting the effectiveness of TLD. Therefore, performing a parametric study, the study is highlighting the effect of this ratio as well as the tuning frequency on structural responses.

2. MODELLING OF TLD WITH EQUIVALENT TMD

In this paper, equivalent amplitude-dependent TMD model developed by Tait *et al*. (2004) is employed to model dynamic behaviour of TLD structure systems. In Tait's approach, the parameters for the model are obtained by matching the energy dissipated by a partially fluid-filled tank with damping screens (TLD) (Figure 1) to an equivalent single-degree-of-freedom (SDOF) TMD. The model is benefiting the research conducted by Yu *et al*. (1999) by changing this assumption that all the fluid mass participates in mass of TLD. In this new approach, the dynamic characteristics of the equivalent TMD including the damper mass, m_{TLD}; the natural frequency of the damper, f_{TLD}; and the inherent damping, ξ_{TLD}, as a function of the excitation amplitude have been assessed conducting a series of shaking-table tests. The experimentally obtained data allow the nonlinear TLD to be modelled as an equivalent amplitude-dependent TMD.

The method is based on matching the energy dissipated by the equivalent TMD (Figure 2) and the estimation of the energy dissipated within the TLD. The amount of energy dissipated by fluid sloshing was evaluated by the measured base shear forces and the corresponding shake table displacements. The energy dissipated by the equivalent TMD, E_{d}, can be expressed in terms of the amplitude of the excitation, A, as

$$E_{\mathrm{d}} = m_{\mathrm{TLD}}(2\pi f)^2 A^2 \pi |H_{z/x}(\beta)| \beta^2 \sin[\theta_{z/x}(\beta)] \tag{1}$$

DOI: 10.1002/tal

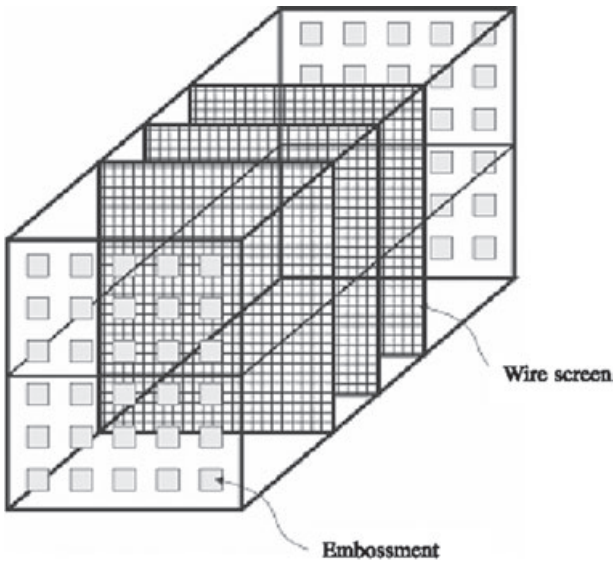

Figure 1. TLD with damping screens (Tait *et al*., 2004)

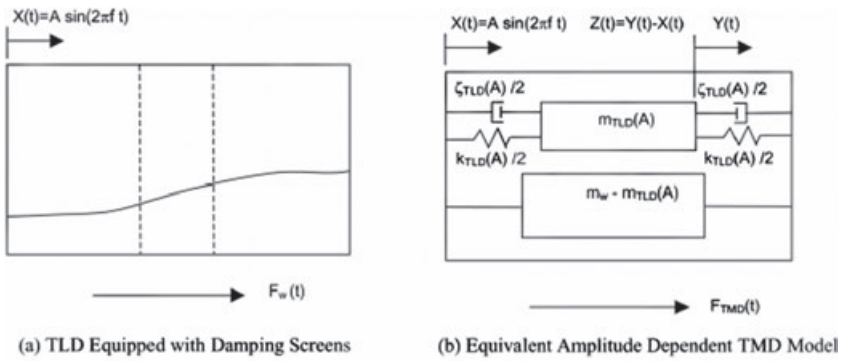

Figure 2. TLD and equivalent TMD model (Tait *et al*., 2004). (a) TLD equipped with damping screens. (b) Equivalent amplitude-dependent TMD model

where $\beta = f / f_{\mathrm{TLD}}$, and f is the excitation frequency. The frequency transfer function, $|H_{z/x}(f)|$, between the TMD relative response motion and the table input motion, $Z(t)$, and also the corresponding phase angle, $\theta_{z/x}$, are obtained by:

$$|H_{z/x}(\beta)| = \frac{1}{\sqrt{(1-\beta^2)^2 + (2\xi_{\mathrm{TLD}}\beta)^2}} \tag{2}$$

$$\tan[\theta_{z/x}(\beta)] = \frac{2\xi_{\mathrm{TLD}}\beta}{1-\beta^2} \tag{3}$$

If the elastic energy for an SDOF system with the mass equal to m_w is defined as

$$E_0 = \frac{1}{2} m_w (2\pi f)^2 A^2 \tag{4}$$

DOI: 10.1002/tal

then normalizing E_d, with E_0, results in

$$E'_d = \frac{E_d}{E_0} = \frac{m_{TLD}}{m_w} |H_{z/x}(\beta)| 2\pi \sin[\theta_{z/x}(\beta)] \tag{5}$$

Using the least square curve-fitting procedure with constraints forcing the theoretical expression, E'_d, to match both the maximum energy dissipated and the total energy dissipated over the range of frequencies tested, the equivalent TMD parameters, m_{TLD}, f_{TLD} and ξ_{TLD}, for all amplitudes of excitation tested have been estimated (Figure 3).

3. MODELLING OF A SHEAR BUILDING EQUIPPED WITH TLD

The TLD structure systems investigated in this study are two-dimensional shear-type structures with n degrees of freedom shown in Figure 4. The TLD is considered to be rectangular installed in any floors. Using the approach described in the previous section, TLD is replaced with an equivalent amplitude-dependent TMD. Assuming small displacements, the equations of motion in the time domain for the TLD structure model illustrated in Figure 4 can be expressed as

$$[m]\{\ddot{u}(t)\} + [c]\{\dot{u}(t)\} + [k]\{u(t)\} = -[m]\{I\}\ddot{u}_g(t) \tag{6}$$

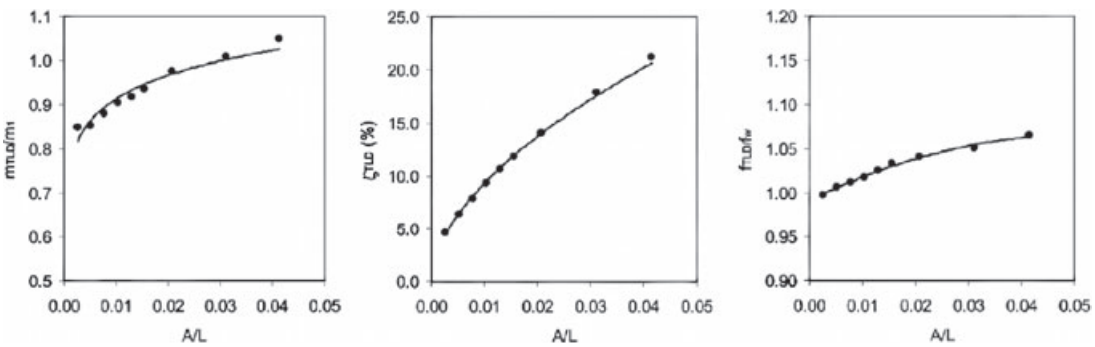

Figure 3. Amplitude-dependent equivalent TMD parameters (Tait *et al*., 2004)

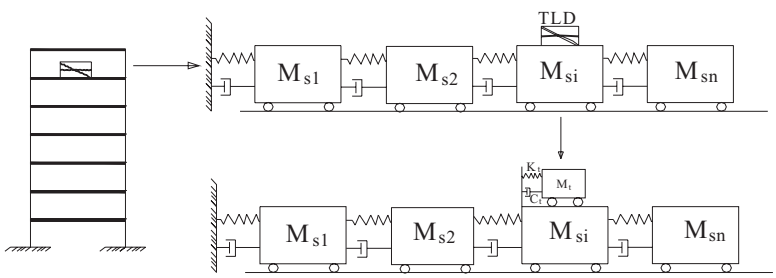

Figure 4. TLD structure model

DOI: 10.1002/tal

in which $[m]$, $[k]$, $[c]$ are the mass, stiffness and damping matrices of the equivalent TMD structure, respectively, and can be expressed as

$$
m_{(n+1)(n+1)} = \begin{bmatrix}
m_{s_1} & 0 & 0 & 0 & 0 & 0 & 0 & 0 \\
 & \cdots & 0 & 0 & 0 & 0 & 0 & 0 \\
 & & m_{s_{j-1}} & 0 & 0 & 0 & 0 & 0 \\
 & & & m_{s_j}+M_0 & & 0 & 0 & 0 \\
 & & & & m_{\mathrm{TLD}} & 0 & 0 & 0 \\
 & & \mathrm{sym} & & & m_{s_{j+1}} & 0 & 0 \\
 & & & & & & \cdots & 0 \\
 & & & & & & & m_{s_n}
\end{bmatrix}
$$

$$
k_{(n+1)(n+1)} = \begin{bmatrix}
k_{1,1} & k_{1,2} & 0 & 0 & 0 & 0 & 0 & 0 \\
 & \cdots & \cdots & 0 & 0 & 0 & 0 & 0 \\
 & & k_{j-1,j-1} & k_{j-1,j} & 0 & 0 & 0 & 0 \\
 & & & k_{j,j}+k_{\mathrm{TLD}} & -k_{\mathrm{TLD}} & k_{j,j+1} & 0 & 0 \\
 & & & & k_{\mathrm{TLD}} & 0 & 0 & 0 \\
 & & \mathrm{sym} & & & k_{j+1,j+1} & k_{j+1,j+2} & 0 \\
 & & & & & & \cdots & \cdots \\
 & & & & & & & k_{n,n}
\end{bmatrix}
\tag{7}
$$

$$
c_{(n+1)(n+1)} = \begin{bmatrix}
c_{1,1} & c_{1,2} & 0 & 0 & 0 & 0 & 0 & 0 \\
 & \cdots & \cdots & 0 & 0 & 0 & 0 & 0 \\
 & & c_{j-1,j-1} & c_{j-1,j} & 0 & 0 & 0 & 0 \\
 & & & c_{j,j}+C_{\mathrm{TLD}} & -C_{\mathrm{TLD}} & c_{j,j+1} & 0 & 0 \\
 & & & & C_{\mathrm{TLD}} & 0 & 0 & 0 \\
 & & \mathrm{sym} & & & c_{j+1,j+1} & c_{j+1,j+2} & 0 \\
 & & & & & & \cdots & \cdots \\
 & & & & & & & c_{n,n}
\end{bmatrix}
$$

In these expressions, m_{TLD}, k_{TLD} and c_{TLD} are the amplitude-dependent equivalent TMD mass, stiffness and damping parameters that vary with the response of its sitting floor, u_{j}. M_0 is the mass of the inside tank water not participating in mass of TLD.

4. SOLVING THE EQUATIONS

Although the structural components of shear buildings are assumed to have the Rayleigh-type damping, however, having taken into account the type of damping emerging from TLDs (amplitude-dependent equivalent TMD), the total damping matrix as a non-classical damping cannot satisfy:

$$[c][m]^{-1}[k] = [k][m]^{-1}[c] \tag{8}$$

To solve the governing equation of motion (Equation (6)), a new iterative approach considering the amplitude-dependent equivalent TMD dynamic parameters based on the complex modal analysis method (Veletsos and Ventura, 1986) is developed. In this method, the complementary solution corresponding to the homogeneous differential equation is obtained by taking

$$\{u(t)\} = \{\psi\} e^{rt} \tag{9}$$

DOI: 10.1002/tal

in which r and $\{\psi\}$ are the eigenvalues and eigenvectors, respectively. Substituting Equation (9) into homogenous differential Equation (6) results in

$$(r^2[m]+r[c]+[k])\{\psi\}=\{0\} \tag{10}$$

Equations of motion in time domain with n coupled equations can be solved with the help of an identity equation (Foss, 1958) as follows:

$$[A]\{\dot{z}\}+[B]\{z\}=\{Y(t)\} \tag{11}$$

where the $2n \times 2n$ matrices $[A]$ and $[B]$ are defined as

$$[A]=\begin{bmatrix}[0] & [m]\\ [m] & [c]\end{bmatrix}_{2n\times 2n},\ [B]=\begin{bmatrix}-[m] & [0]\\ [0] & [k]\end{bmatrix}_{2n\times 2n} \tag{12}$$

and the $2n \times 1$ state vectors $\{z\}$ and $\{Y(t)\}$ are

$$\{z\}=\begin{Bmatrix}\{\dot{u}\}\\ \{u\}\end{Bmatrix},\quad \{Y(t)\}=\begin{Bmatrix}0\\ -[m]\{I\}\ddot{u}_g(t)\end{Bmatrix} \tag{13}$$

To decouple Equation (11), the eigenvectors of the eigenvalue problem associated with the equation similar to Equation (9) by taking

$$\{z\}=\{Z\}e^{rt} \tag{14}$$

are used. The associated eigenvalue problem is

$$(r[A]+[B])\{Z\}=\{0\} \tag{15}$$

where

$$\{Z\}=\begin{Bmatrix}r\{\psi\}\\ \{\psi\}\end{Bmatrix} \tag{16}$$

Therefore, for the given eigenvalue problem, there are n complex eigenvalue couples, $(r_j,\bar{r}_j)$ and n complex eigenvector couples, $(\{\psi_j\},\{\overline{\psi}_j\})$ as follows:

$$\begin{Bmatrix}r_j\\ \bar{r}_j\end{Bmatrix}=-q_j\pm i\tilde{p}_j,\quad \begin{Bmatrix}\{\psi_j\}\\ \{\overline{\psi}_j\}\end{Bmatrix}=\{\phi_j\}\pm i\{\chi_j\} \tag{17}$$

where

$$\begin{Bmatrix}r_j\\ \bar{r}_j\end{Bmatrix}=-\zeta_j p_j\pm i\tilde{p}_j,\ p_j=\sqrt{(q_j^2+\tilde{p}_j^2)},\quad \tilde{p}_j=p_j\sqrt{1-\zeta_j^2} \tag{18}$$

Comparing these equations with the governing motion equation for damped SDOF systems, it can be concluded that p_j, $\tilde{p}_j$ and $\{\phi_j\}$ are the undamped natural frequency, damped natural frequency and mode shape corresponding to the jth natural frequency of the structure, respectively. Using linear combina-

DOI: 10.1002/tal

tion of complex eigenvalue couples and their corresponding complex eigenvector couples, the modal displacements for the *j*th mode shape can be obtained by

$$\{u_j(t)\} = 2\,\mathrm{Re}\left\lfloor C_j\{\psi_j\}e^{r_j t}\right\rfloor \tag{19}$$

and therefore by combination of all modes, the structural response will be calculated as

$$\{u(t)\} = 2\sum_{j=1}^{n}\mathrm{Re}\left[C_j\{\psi_j\}e^{r_j t}\right] \tag{20}$$

In order for the TLD to be modelled as amplitude-dependent TMD, the structural response is calculated using an iterative procedure in which the equivalent TMD properties in each iteration are updated. In the first step, an initial value of the structural displacements for the structure without TLD is made, allowing the parameters of the equivalent TMD to be obtained from the equivalent amplitude-dependent TMD model developed by Tait *et al*. (2004). Subsequently, the equations of motion for the structure with TLD are solved, and a new estimate of the structural displacements is calculated leading to new values of the equivalent TMD properties to be used in the next iteration. The iterative analyses are continued until the solution is converged.

5. NUMERICAL EXAMPLES

The feasibility of the numerical approach for multi-degree of freedom (MDOF) structures equipped with TLDs is numerically examined in this section. A 10-storey frame building (structure 'A') with the natural fundamental period about 2 seconds described in Sadek and Mohraz (1998), a nine-storey shear building having natural fundamental period of 1·25 seconds (structure 'B') and Nanjing TV tower structure described by Li *et al*. (2004) with the natural fundamental period of 2·94 seconds shown in Figure 5 (structure 'C') are employed as three numerical practical examples for controlling the seismic responses of MDOF structures by use of TLDs with screens, and demonstrating the vibration reduction effectiveness of the proposed idea. The physical parameters of the mentioned structures are summarized in Table 1. Three model structures with and without TLD were subjected to 90º component of Arleta and 90º component of Santamonica stations from the Northridge earthquake (1994), the 90º component of the Corralitos Station from the Loma Prieta earthquake (1989) and the 90º component of the Takatori Station from the Kobe earthquake (1995); each scaled to a peak ground acceleration of 0·4 *g* (Table 2 and Figure 6).

Assuming that the TLD is placed on the roof of the structure for suppressing the vibration induced by earthquakes, the mass ratio of TLD is computed as the ratio of liquid mass to the generalized mass of the structure, i.e. $\mu = \rho AL/\phi_1^T[M]\phi_1$, where $[M]$ is the structural mass matrix and ϕ_1 is the fundamental mode shape normalized to have a unit participation factor. For all three structures considered, the modal masses with modal natural periods for up to fifth mode shape are shown in Table 3. Design of TLDs is followed by selection of the mass ratio ($\overline{m} = m_{\mathrm{TLD}}/m$) first and the remaining parameters are determined accordingly. To examine the effectiveness of the TLD in reduction of the structural response, the ratio of the response for the structure with TLD and the structure without TLD is defined as

$$\Psi(X) = \frac{X_{\text{With TLD}}}{X_{\text{Without TLD}}}\times 100\% \tag{21}$$

DOI: 10.1002/tal

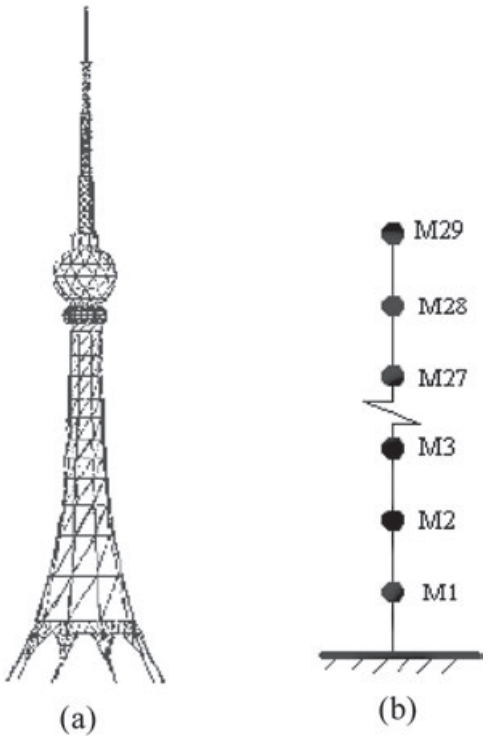

Figure 5. TV tower model used as structure 'C'. (a) Tower Structure, (b) Lumped mass system

in which X is response of the structure including the roof displacement and base shear. To better understand the effectiveness of TLDs on the structural response, the root-mean-square (RMS) of the response Fourier amplitude is also calculated. Ψ' represents the ratio of the RMS of the response for the structure with and without TLD as

$$\Psi'(X) = \frac{RMS \text{ of } FFT(X_{\text{With TLD}})}{RMS \text{ of } FFT(X_{\text{Without TLD}})} \times 100\% \tag{22}$$

In the first step, the optimum mass ratio is selected throughout a set of parametric analyses by tuning the natural frequency of TLD to the first natural fundamental frequency of the structure ($\Omega = 1$). For the structures 'A', 'B' and 'C', the optimum mass ratios were obtained as 4, 4 and 3%, respectively. To select the optimum tuning ratio, Ω, and then the liquid tank dimensions, different ratios ranging from 0·5 to 1·6 were used in the analyses, and the optimum ratios for different structures were evaluated (Tables 4–7). For the structure 'C', due to this fact that the first mode shape corresponding to the vibration of antenna has less affect to the overall structural response, and the second mode shape makes a great contribution to seismic response of the system, the main objective was to control vibration of the second mode. The structures were analysed using the method described above subjected to the different ground deformations assumed in this study. Figures 7 and 8 show the variation of the reduction factor of the roof displacement and base shear for the structure 'A' with tuning frequency ratio. For this structure, the variations of roof RMS displacement ratio and RMS base shear ratio with

DOI: 10.1002/tal

Table 1. Physical parameters of the structure

	Structure A			Structure B			Structure C			
DOF	M (ton)	K (KN/m)	ξ (mode)	M (ton)	K (ton/m)	ξ (mode)	M (kg)	L (m)	I (m^4)	ξ (mode)
1	179	62·47	0·02	140	11 000	0·02	20 682	22·5	63·129	0·02
2	170	59·26	0	130	11 000	0·02	61 324	17·5	29·419	0·02
3	161	56·14	0	130	11 000	0·02	46 121	15	16·89	0·02
4	152	53·02	0	130	11 000	0·02	35 166	13	11·348	0·02
5	143	49·91	0	130	11 000	0·02	26 649	9·4	8·975	0·02
6	134	46·79	0	130	11 000	0·02	24 343	8·6	7·562	0·02
7	125	43·67	0	110	10 000	0·02	19 682	7·8	6·581	0·02
8	116	40·55	0	110	10 000	0·02	15 469	7·4	3·747	0·02
9	107	37·43	0	110	10 000	0·02	14 734	7·1	3·378	0·02
10	98	34·31	0				14 022	6·7	3·031	0·02
11							13 519	6·4	2·812	0·02
12							13 156	6·2	2·664	0·02
13							10 766	6·1	2·523	0·02
14							18 128	4	2·176	0·02
15							16 852	3·8	1·371	0·02
16							23 154	3·4	1·328	0·02
17							45 356	4·7	1·277	0·02
18							59 522	5·7	1·04	0·02
19							45 178	6	0·984	0·02
20							21 879	4·8	0·931	0·02
21							14 443	4·2	0·887	0·02
22							14 075	13	0·434	0·02
23							13 588	9	0·321	0·02
24							13 262	12	0·094	0·02
25							10 023	12	0·094	0·02
26							6 734·2	11	0·026	0·02
27							5 200·5	10	0·019	0·02
28							4 400·6	12	0·004	0·02
29							1 202·3	11	0·001	0·02
Sum	1385			1120			628 630·6	260·3		

Table 2. Ground excitation parameters

Record name	Station—direction	PGA (g)	PGV (cm/s)	PGD (cm)	Used PGA (g)	Duration (s)
Northridge (1994)	Arleta—90	0·344	40·6	15·04	0·4	24·7
Northridge (1994)	Santamonica—90	0·883	41·7	15·09	0·4	9·8
Loma Prieta (1989)	Corralitos—90	0·479	45·2	11·37	0·4	17·9
Kobe (1995)	Takatori—90	0·615	120·7	32·72	0·4	14·5

DOI: 10.1002/tal

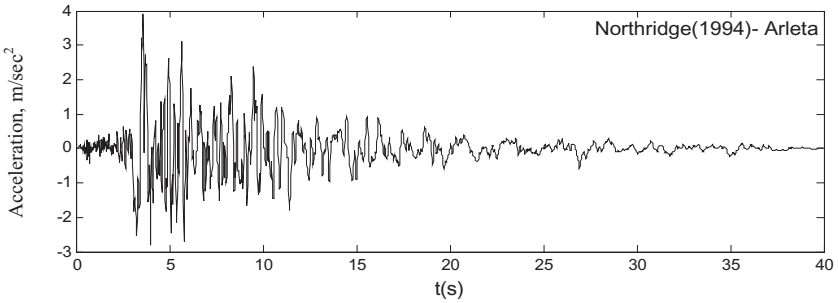

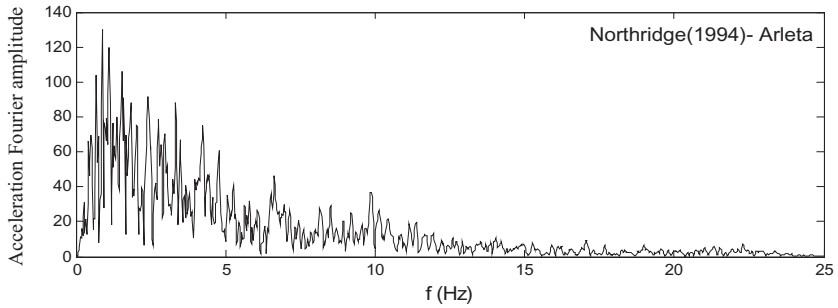

a) Northridge Earthquake (Arleta)

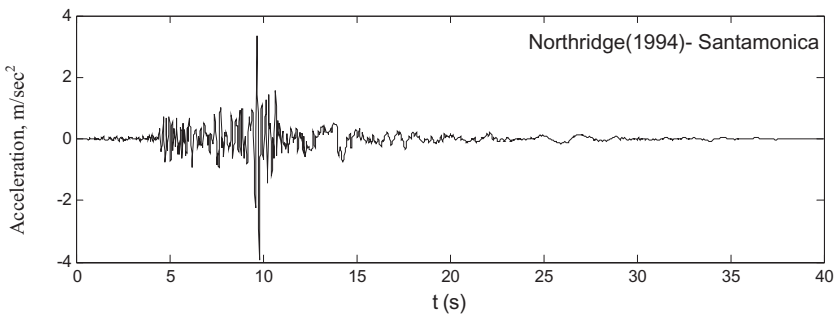

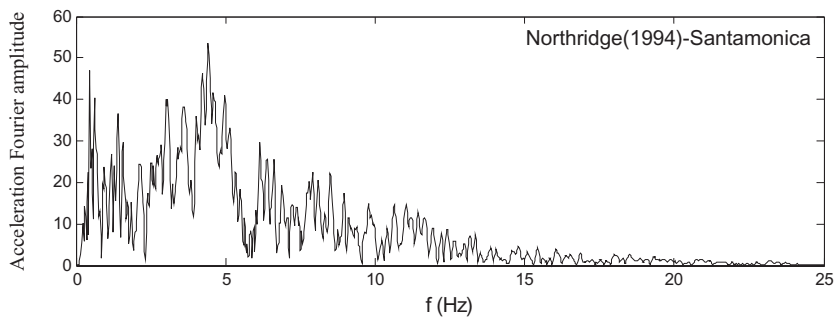

b) Northridge Earthquake (Santamonica)

Figure 6. Earthquake excitations used in this study. (a) Northridge earthquake (Arleta), (b) Northridge earthquake (Santamonica)

DOI: 10.1002/tal

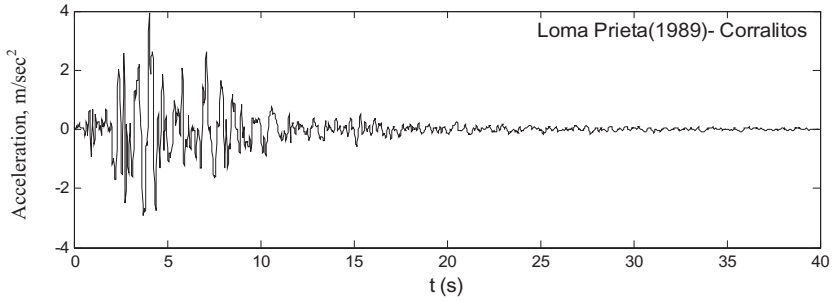

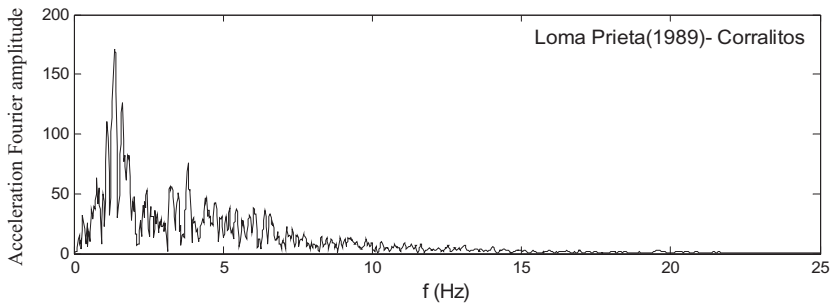

c) Loma Prieta Earthquake (Corralitos)

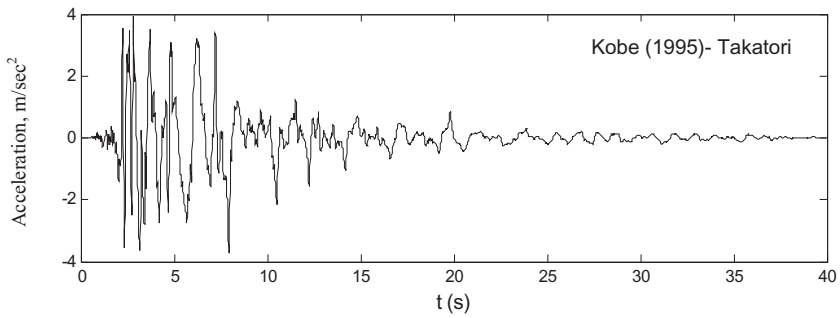

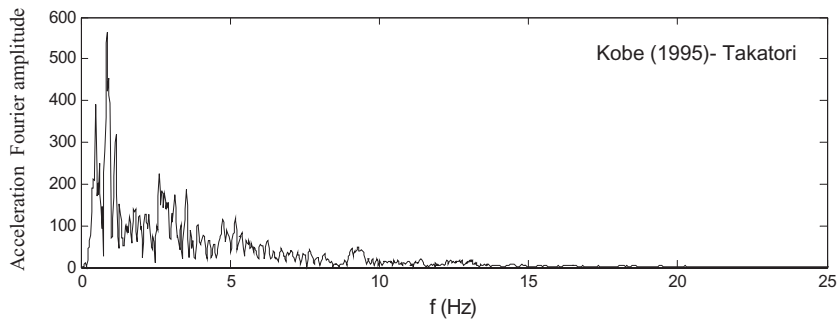

d) Kobe Earthquake (Takatori)

Figure 6. (c) Loma Prieta earthquake (Corralitos), (d) Kobe earthquake (Takatori)

DOI: 10.1002/tal

Table 3. Modal parameters of the structures

Structure	A			B			C		
Mode	T (s)	f (Hz)	Effective mass (ton)	T (s)	f (Hz)	Effective mass (ton)	T (s)	f (Hz)	Effective mass (ton)
(1)	1·99	0·50	1108·9	1·25	0·79	946·17	2·94	0·34	27·74
(2)	0·75	1·32	163·01	0·43	2·29	104·01	1·74	0·57	69·38
(3)	0·46	2·15	57·14	0·26	3·70	38·9	1·40	0·71	61·71
(4)	0·34	2·93	26·70	0·19	5·09	17·35	1·12	0·88	350·37
(5)	0·27	3·65	14·08	0·16	6·28	7·60	0·83	1·20	31·2

Table 4. TLD parameters used for structure ‘A’

Ω	0·39	0·49	0·6	0·7	0·74	0·79	0·85	0·9	0·95	1	1·047	1·1	1·14	1·15	1·2	1·24	1·3	1·4	1·51	1·6	1·69
L	2·5	2	2	1·4	1·45	1·5	1·5	1·5	1·5	1·5	1·5	1·5	1·4	1·35	1·35	1·35	1·35	1·2	1·15	1	1
h	0·1	0·1	0·15	0·1	0·12	0·15	0·175	0·2	0·22	0·25	0·28	0·32	0·3	0·28	0·32	0·35	0·4	0·38	0·45	0·37	0·5
T_w	2·06	4·05	3·32	2·8	2·7	2·5	2·34	2·2	2·09	2	1·9	1·81	1·74	1·73	1·64	1·6	1·5	1·42	1·32	1·24	1·18
h/L	0·04	0·05	0·07	0·07	0·083	0·1	0·11	0·133	0·15	0·167	0·18	0·21	0·214	0·2	0·23	0·26	0·29	0·31	0·39	0·37	0·5

Table 5. TLD parameters used for structure ‘B’

Ω	0·7	0·75	0·8	0·85	0·9	0·95	1	1·05	1·1	1·15	1·2	1·25
L	1·7	1·5	1·2	1·06	0·9	0·93	0·8	0·8	0·8	0·78	0·7	0·7
h	0·45	0·41	0·28	0·25	0·2	0·25	0·2	0·23	0·28	0·3	0·26	0·32
T_w	1·78	1·66	1·57	1·46	1·38	1·31	1·25	1·19	1·13	1·09	1·04	1
h/L	0·26	0·27	0·23	0·32	0·22	0·26	0·25	0·29	0·35	0·38	0·37	0·45

Table 6. TLD parameters used for structure ‘C’ to control the first mode

Ω_1	0·7	0·75	0·8	0·85	0·9	0·95	1	1·05	1·1	1·15	1·2	1·25	1·3
L (m)	7·5	6·8	6·1	5·5	5	4·1	4	3·5	3·45	3	2·7	2·7	2·7
h (m)	1·48	1·4	1·3	1·2	1·1	0·8	0·866	0·73	0·8	0·65	0·57	0·63	0·7
T_w (s)	4·17	3·91	3·65	3·44	3·27	3·1	2·94	2·79	2·66	2·54	2·44	2·35	2·27
h/L	0·2	0·2	0·21	0·22	0·22	0·2	0·22	0·21	0·23	0·21	0·21	0·23	0·26
Ω_2	0·4	0·44	0·48	0·5	0·53	0·56	0·59	0·62	0·65	0·68	0·71	0·74	0·77
Ω_3	0·32	0·36	0·38	0·4	0·42	0·45	0·47	0·5	0·52	0·55	0·57	0·59	0·61
Ω_4	0·26	0·28	0·3	0·32	0·34	0·36	0·38	0·4	0·42	0·44	0·46	0·48	0·49

Table 7. TLD parameters used for structure ‘C’ to control the second mode

Ω_2	0·7	0·75	0·8	0·85	0·9	0·95	1	1·05	1·1	1·15	1·2	1·25	1·3	1·4	1·49
L (m)	2·5	2·5	1·9	1·8	1·6	1·5	1·4	1·3	1·2	1·1	1	0·95	0·9	0·85	0·8
h (m)	0·46	0·55	0·35	0·36	0·32	0·31	0·3	0·29	0·28	0·25	0·23	0·22	0·22	0·24	0·25
T_w (s)	2·45	2·31	2·16	2·03	1·91	1·83	1·74	1·66	1·56	1·51	1·43	1·39	1·33	1·23	1·11
h/L	0·18	0·22	0·18	0·2	0·2	0·2	0·21	0·22	0·23	0·22	0·23	0·23	0·24	0·28	0·31

DOI: 10.1002/tal

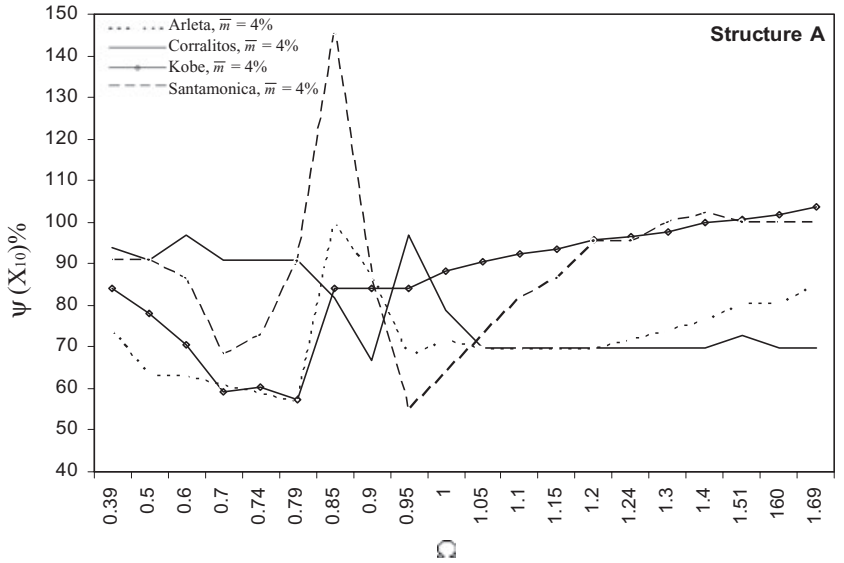

Figure 7. Variation of roof displacement ratio with tuned frequency ratio (structure 'A')

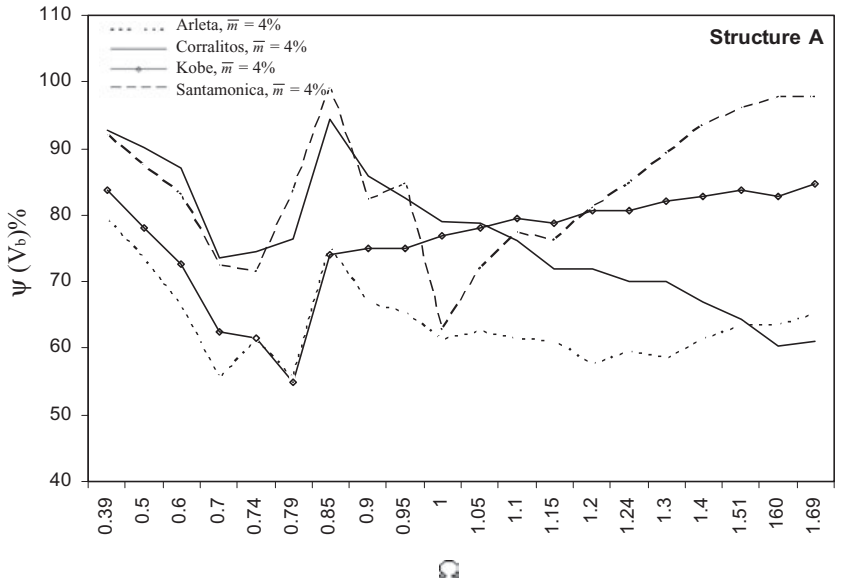

Figure 8. Variations of base shear ratio with tuned frequency ratio (structure 'A')

tuning frequency ratio are also plotted in Figures 9 and 10. As it can be noted from these figures, for structure 'A', the tuning frequency ratios equal to 0·79, 0·9, 0·79 and 0·95 can be selected as the optimum tuning frequency ratio for Arleta, Corralitos, Kobe and Santamonica excitations, respectively. To get an insight about the effect of mass ratio on the seismic response of shear buildings equipped with TLDs, the analyses were repeated for the TLD structure system tuned to the optimum tuning frequencies having different mass ratios subjected to different base inputs. The variations of

DOI: 10.1002/tal

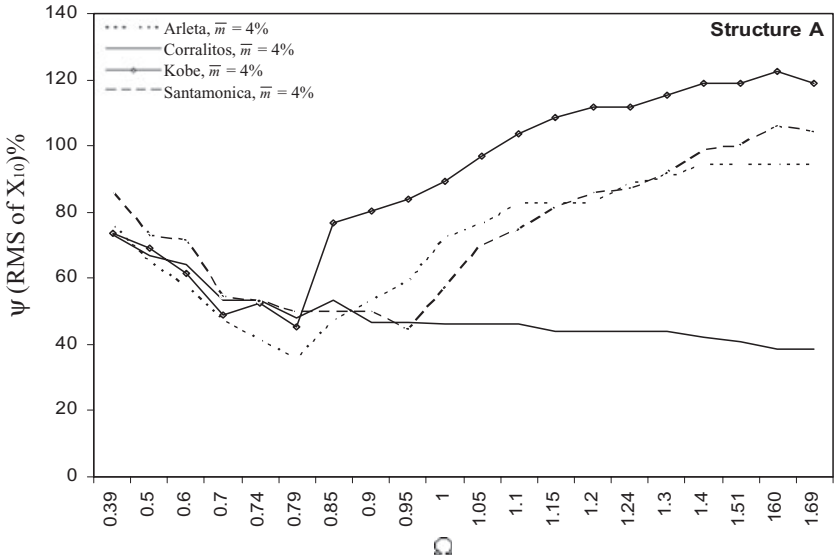

Figure 9. Variation of roof RMS displacement ratio with tuned frequency ratio (structure 'A')

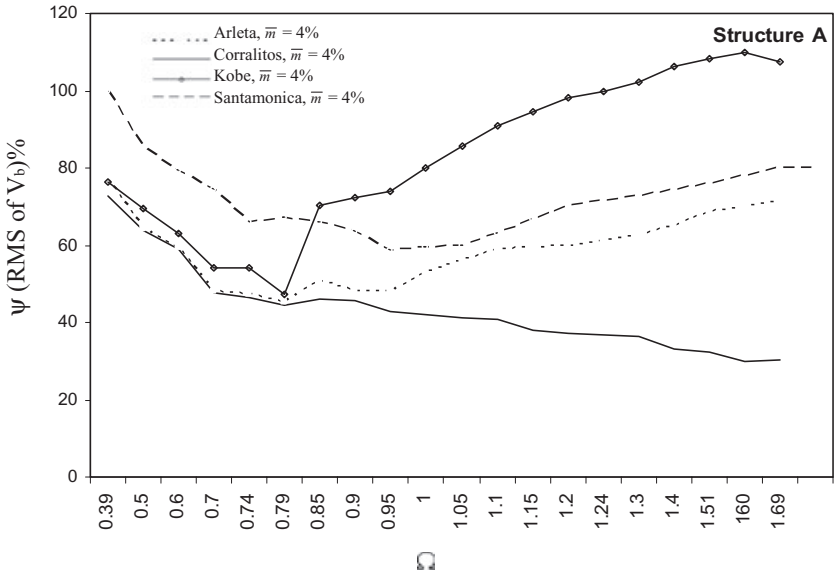

Figure 10. Variation of RMS base shear ratio with tuned frequency ratio (structure 'A')

the roof displacement and base shear ratios, and their RMS with mass ratio are given in Figures 11–14. The results of the displacements obtained from analyses performed for structure 'A' equipped with the TLD having parameters described above are summarized in Table 8. As it can be noted, the results show a reduction of up to 38% in displacements. The roof displacements of the structure with no control and with TLD to the two ground excitations of Arleta and Corralitos are plotted in Figures 15 and 16. The figures show that the effectiveness of TLD is significant. From Fourier

DOI: 10.1002/tal

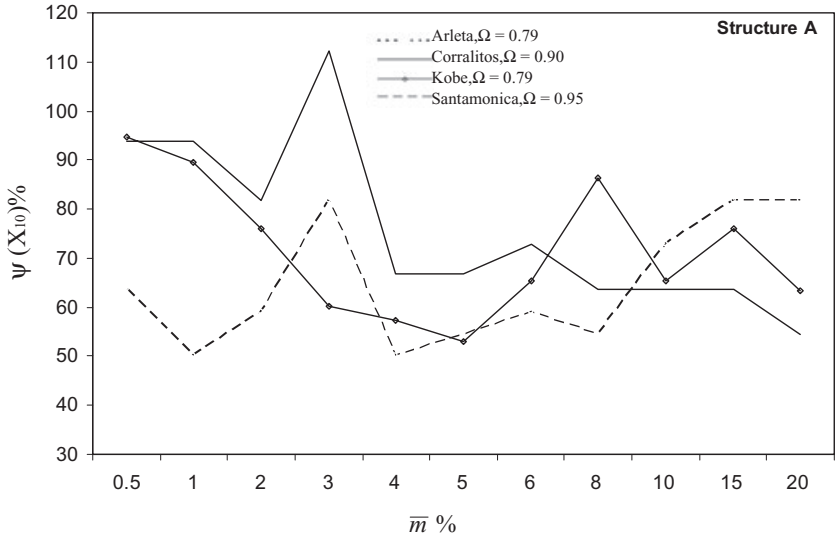

Figure 11. Variation of roof displacement ratio with tuned mass ratio (structure 'A')

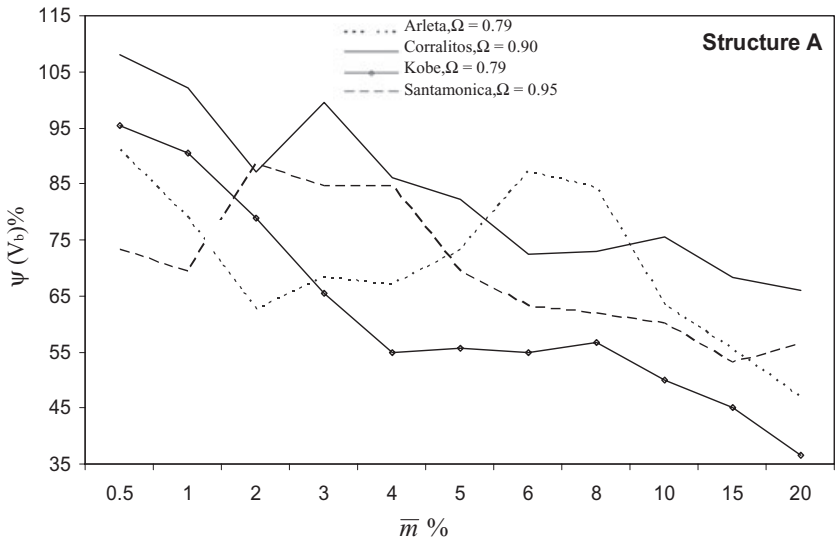

Figure 12. Variation of base shear ratio with tuned mass ratio (structure 'A')

spectrum of the response, it can also be noted that as TLD introduces one more degree of freedom, the fundamental natural frequency is shifted from 0·5 Hz to frequencies of 0·43 and 0·55 Hz. Also, depending on the frequency content of excitation, the reduction to the response of the structure is different. Figures 17 and 18 show that for Arleta record, the structure with TLD results in remarkable reduction in the base shear response while for Corralitos earthquake, the reduction is not as significant. The maximum floor displacements for the structure without TLD

DOI: 10.1002/tal

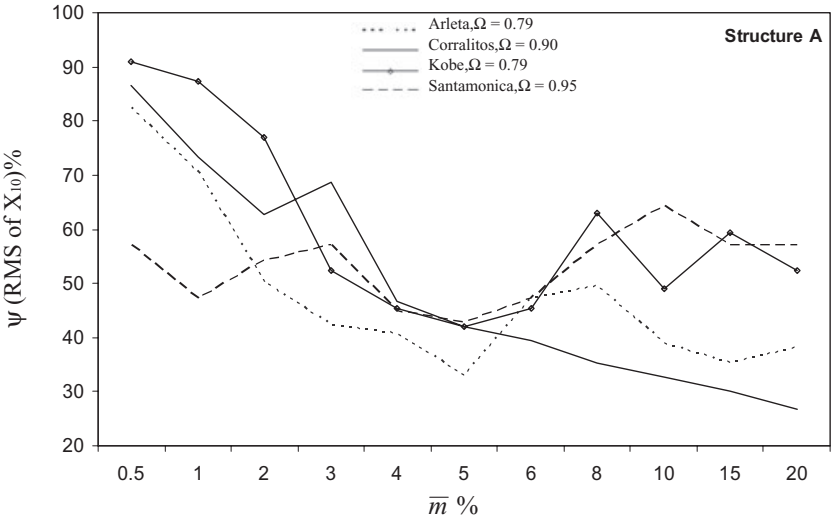

Figure 13. Variation of roof RMS displacement ratio with tuned mass ratio (structure 'A')

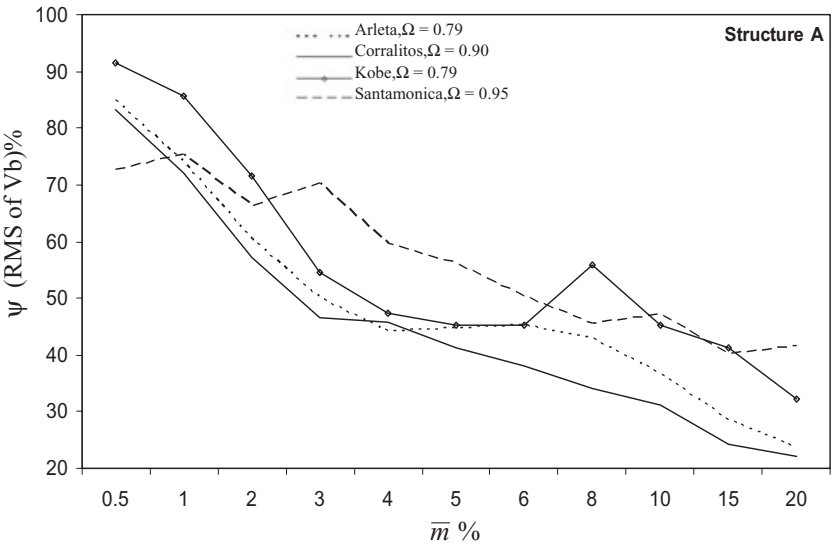

Figure 14. Variation of RMS base shear ratio with tuned mass ratio (structure 'A')

DOI: 10.1002/tal

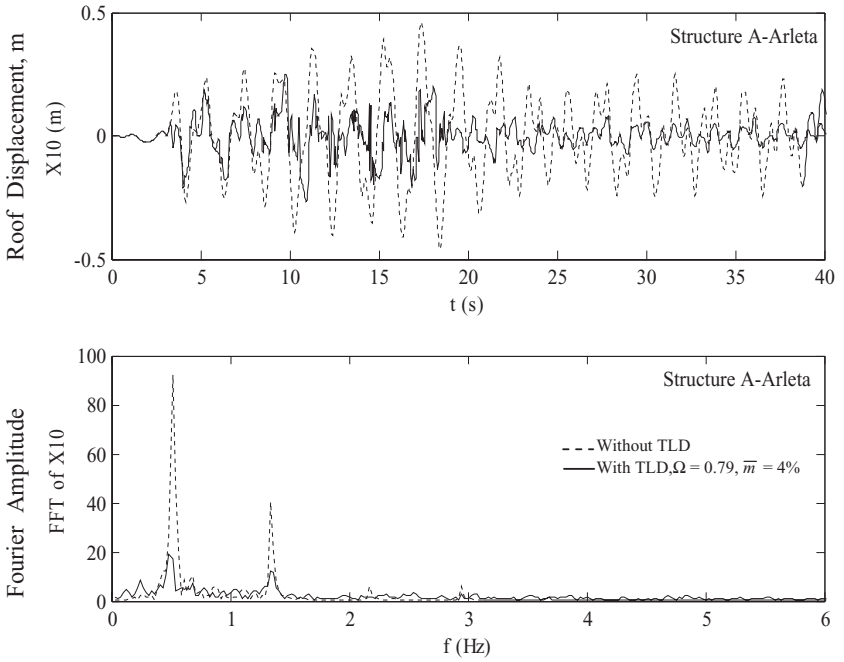

Figure 15. Roof displacement time history and Fourier amplitude of structure 'A' with and without TLD subjected to Northridge (Arleta) earthquake

Table 8. Maximum displacements of the 10-storey shear building (structure 'A') with and without TLD

Northridge—Arleta—0·4 g, structure 'A'			Loma Prieta—Capitola—0·4 g, structure 'A'		
	No control	With TLD		No control	With TLCD
DOF	X_{10} (m)	X_{10} (m)	DOF	X_{10} (m)	X_{10} (m)
1	0·0814	0·0534	1	0·0721	0·0523
2	0·1533	0·0979	2	0·1223	0·0911
3	0·2179	0·1315	3	0·1371	0·1006
4	0·2745	0·1525	4	0·1520	0·1052
5	0·3112	0·1668	5	0·1594	0·1164
6	0·3373	0·1769	6	0·1820	0·1477
7	0·3558	0·2075	7	0·1980	0·1215
8	0·4135	0·2454	8	0·2043	0·1523
9	0·4448	0·2712	9	0·2148	0·1608
10	0·4626	0·2853	10	0·2577	0·1712

and the structure with TLD tuned to the optimum tuning frequency using different mass ratios are presented in Figure 19.

Similar parametric analyses were also performed for structures 'B' and 'C'. However, for structure 'C' as it was stated, the first mode is corresponding to the antenna vibration and has less contribution to the overall seismic response. In contrast, the second mode plays an important role in the seismic response of the tower. Hence, the approach presented here was used for controlling the dynamic response of the structure placing the TLD on the 20th degree of the freedom at the top of the observa-

DOI: 10.1002/tal

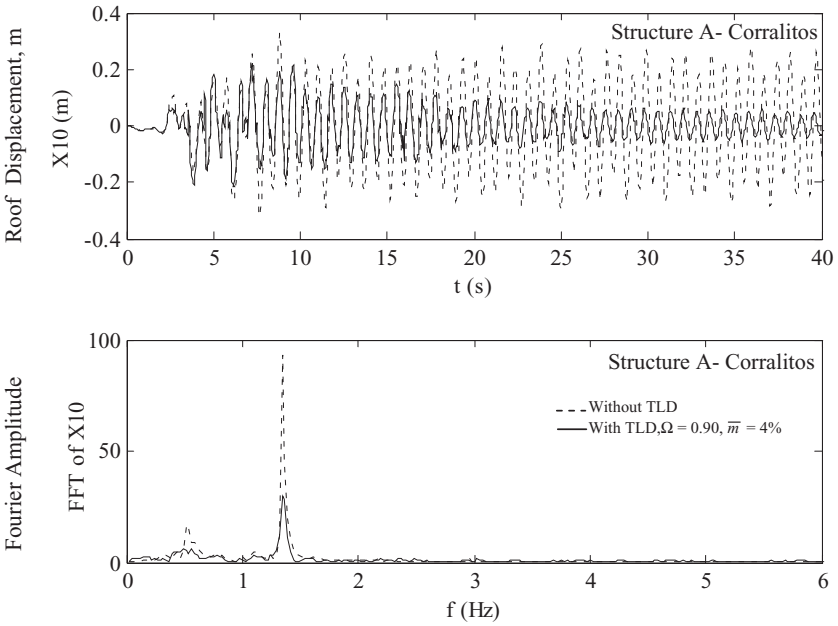

Figure 16. Roof displacement time history and Fourier amplitude of structure 'A' with and without TLD subjected to Loma Prieta earthquake

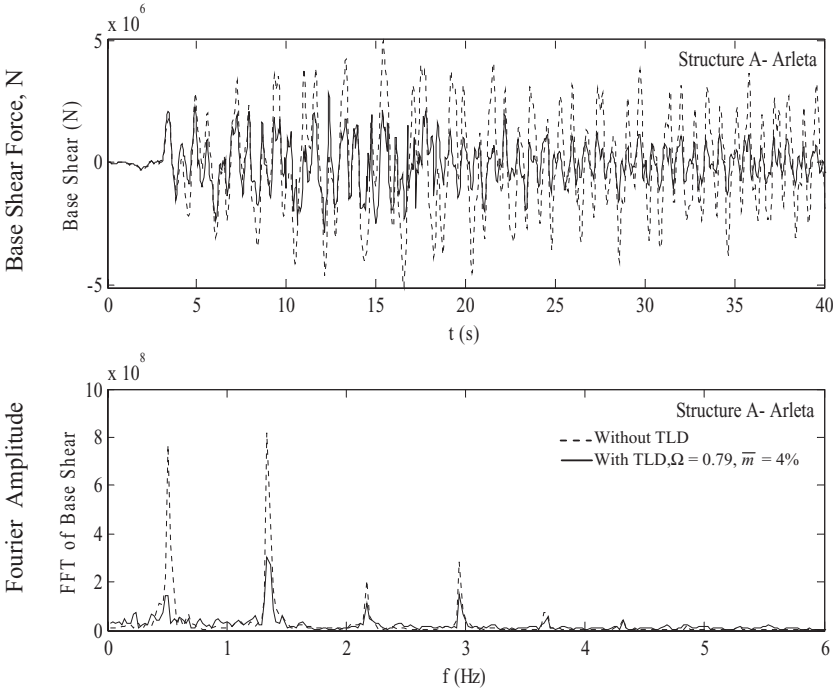

Figure 17. Base shear force time history and Fourier amplitude of structure 'A' with and without TLD subjected to Northridge (Arleta) earthquake

DOI: 10.1002/tal

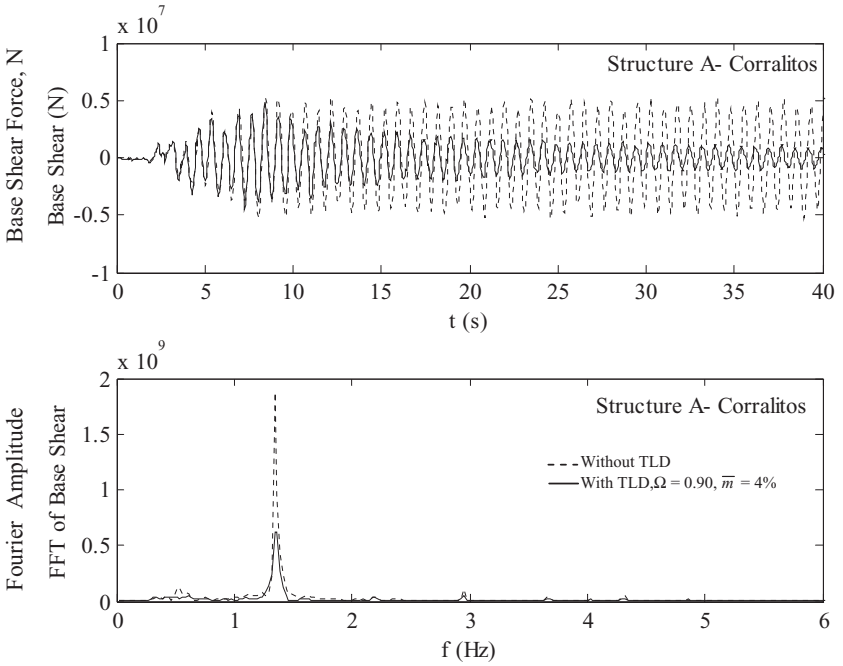

Figure 18. Base shear force time history and Fourier amplitude of structure 'A' with and without TLD subjected to Loma Prieta earthquake

tion deck (Figure 5). The variations of displacement and base shear reduction parameters, to their Fourier Amplitude RMS with tuning frequency ratio using the trail optimum mass ratio for structures 'B' and 'C' are plotted in Figures 20–23 and Figures 24–27, respectively. It can be seen from the results that the tuning frequency ratios equal to 0·85, 0·85, 0·85 and 1·0 for structure 'B', and 2, 1·30, 1·10 and 1·40 for structure 'C' could be chosen as the optimum tuning frequency ratios for Arleta, Corralitos, Kobe and Santamonica excitations, respectively. Similar to structure 'A' throughout a parametric study emphasizing the mass ratio, the analyses were repeated for structures 'B' and 'C' equipped with TLD tuned to the optimum tuning frequencies obtained from the last step subjected to different ground excitations. The variations of the roof displacement and base shear ratios, and their RMS with mass ratio are given in Figures 28–31 for structure 'B', and in Figures 32–35 for structure 'C'. The maximum floor displacements of structures 'B' and 'C' without TLD and with TLD tuned to the optimum tuning frequency and for a range of practical mass ratios subjected to the assumed earthquakes in this paper are presented in Figures 36 and 37.

6. CONCLUSIONS

The objective of this study was to provide a clear understanding of the seismic behaviour of structures having TLD with screens attached. Replacing TLDs with some amplitude-dependent TMDs, a complex modal analysis formulation for seismic response of shear structures equipped with TLD having internal screens, has been presented. A recently new technique based on some experimentally obtained data was used to determine the amplitude-dependent parameters of equivalent TMDs, m_{TLD}, ξ_{TLD} and f_{TLD}. In the proposed approach, the structure response is calculated using an iterative procedure where the equivalent TMD properties are updated until the solution is converged. The implementation of this

DOI: 10.1002/tal

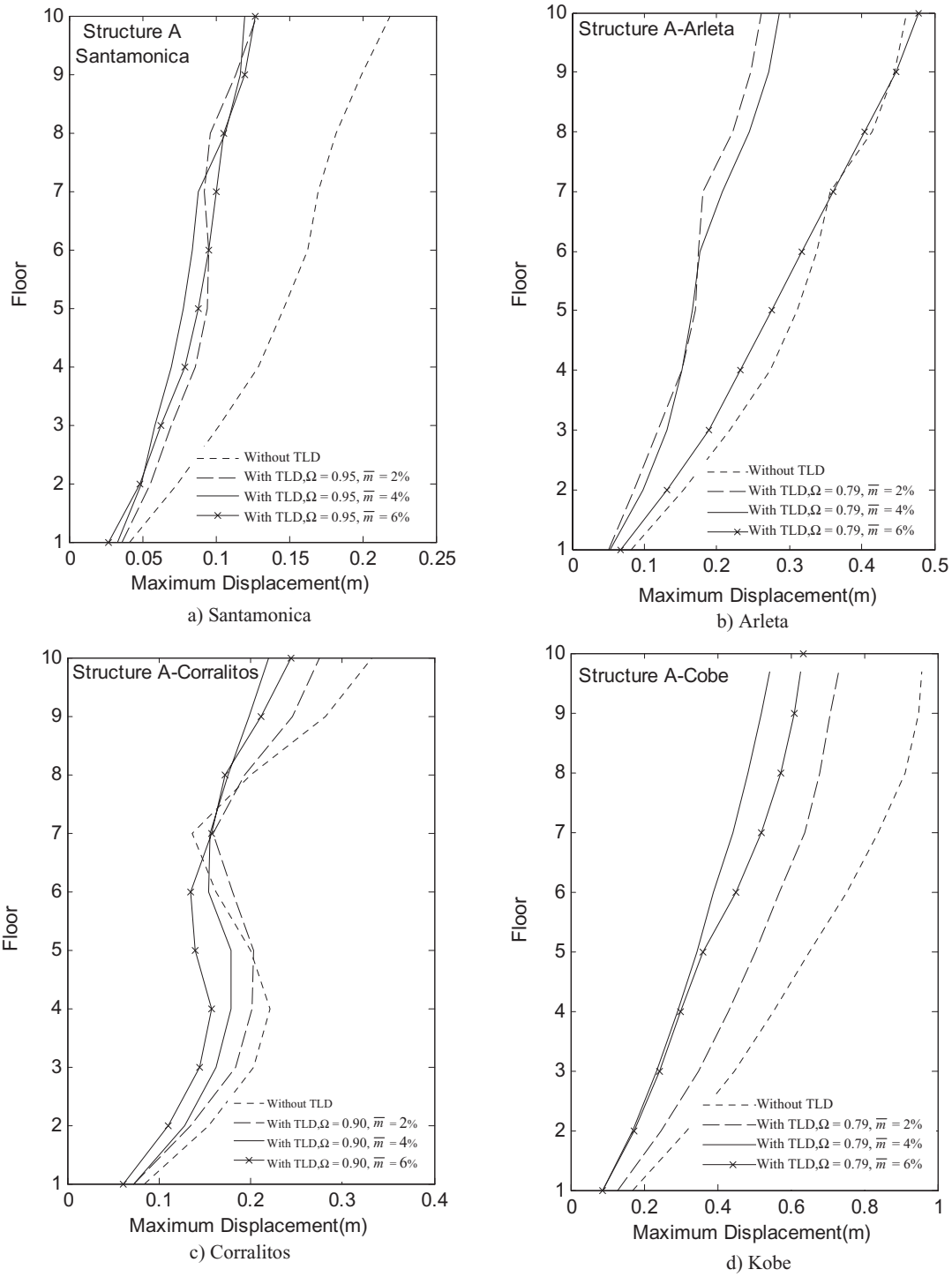

Figure 19. Variation of maximum floor displacements for different tuned mass ratios (structure 'A'): (a) Santamonica, (b) Arleta, (c) Corralitos and (d) Kobe

DOI: 10.1002/tal

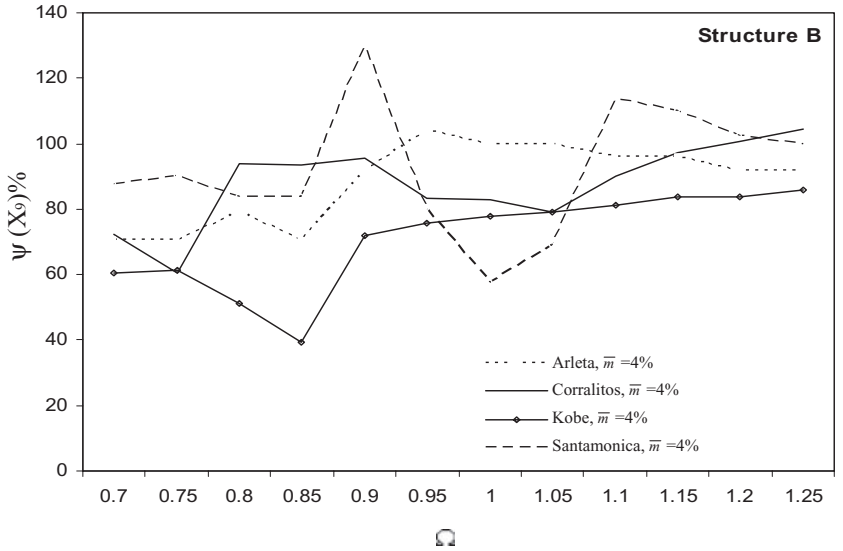

Figure 20. Variation of roof displacement ratio with tuned frequency ratio (structure 'B')

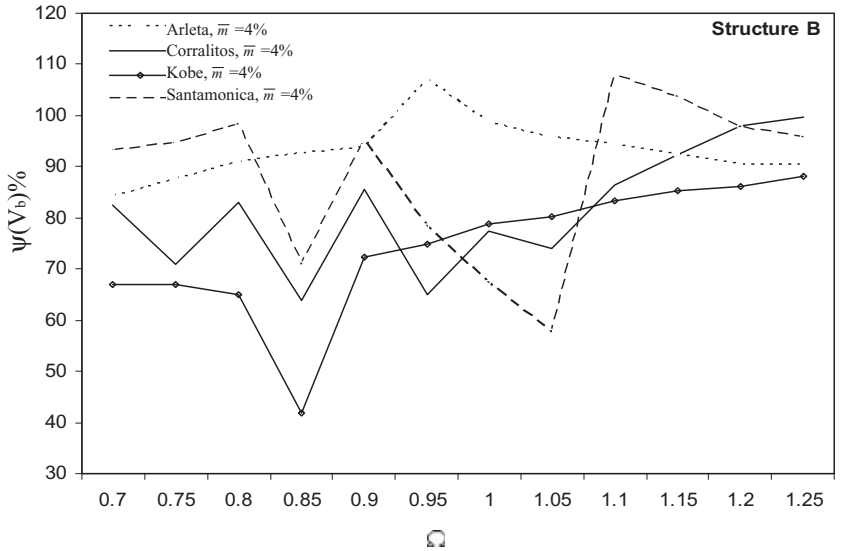

Figure 21. Variations of base shear ratio with tuned frequency ratio (structure 'B')

DOI: 10.1002/tal

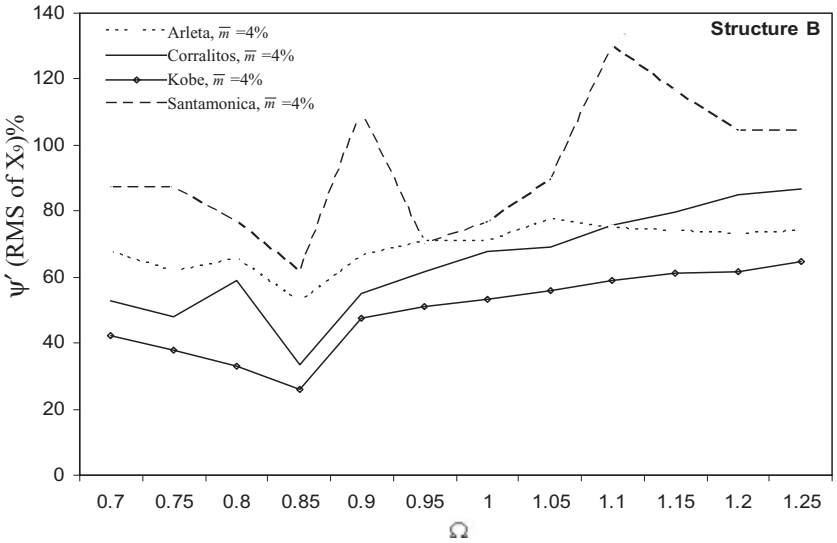

Figure 22. Variation of roof RMS displacement ratio with tuned frequency ratio (structure 'B')

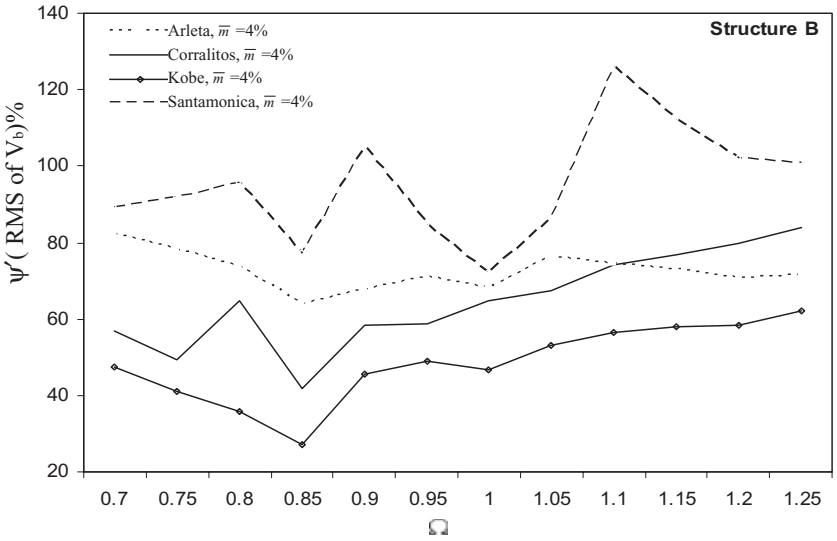

Figure 23. Variation of RMS base shear ratio with tuned frequency ratio (structure 'B')

DOI: 10.1002/tal

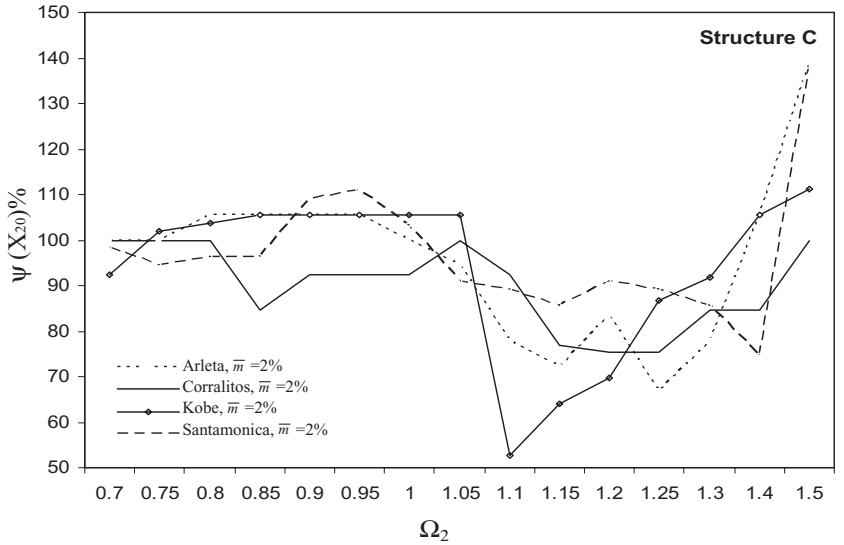

Figure 24. Variation of the 20th mass displacement ratio with tuned frequency ratio (structure 'C')

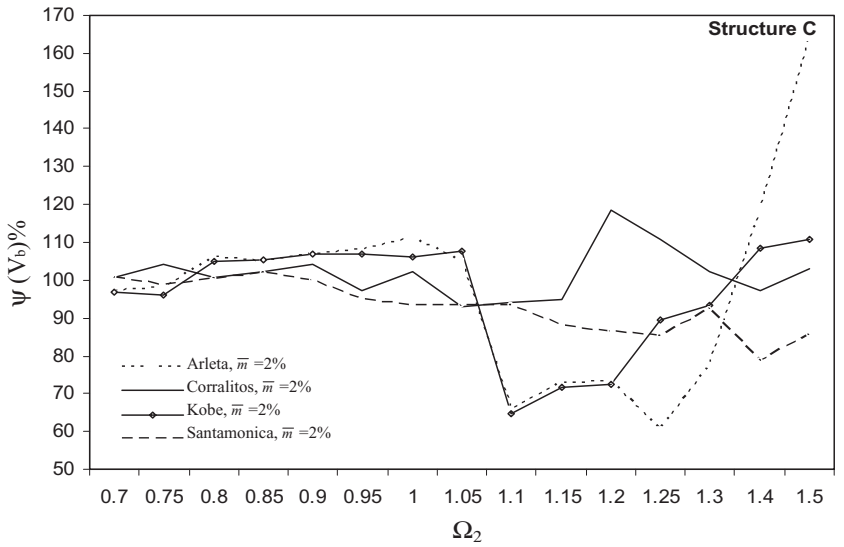

Figure 25. Variation of base shear ratio with tuned frequency ratio (structure 'C')

DOI: 10.1002/tal

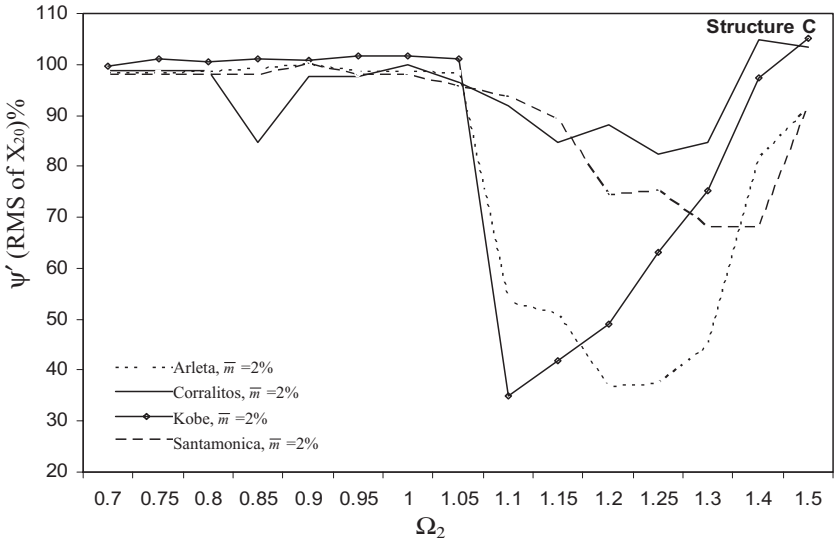

Figure 26. Variation of RMS of the 20th mass displacement ratio with tuned frequency ratio (structure 'C')

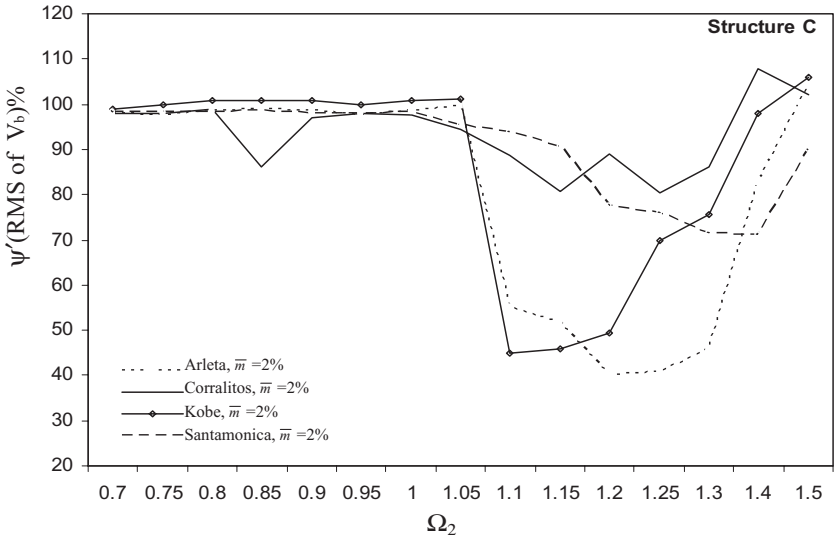

Figure 27. Variation of RMS base shear ratio with tuned frequency ratio (structure 'C')

DOI: 10.1002/tal

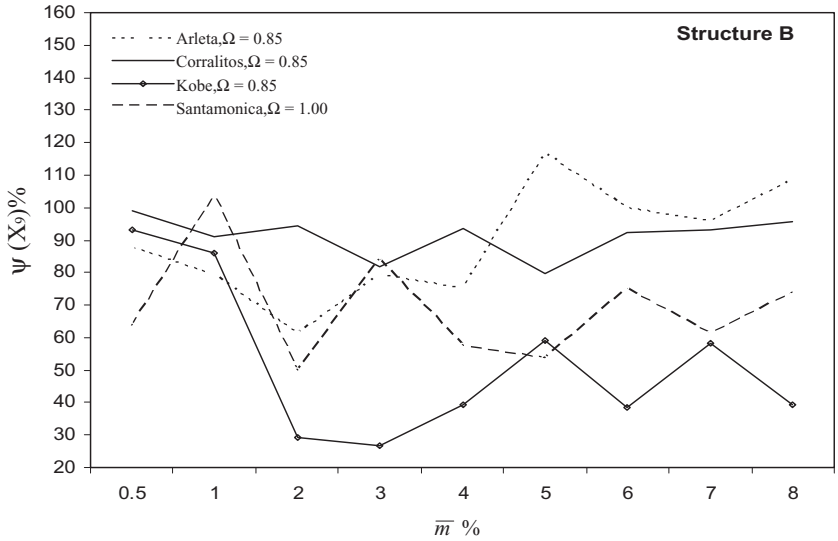

Figure 28. Variation of roof displacement ratio with tuned mass ratio (structure 'B')

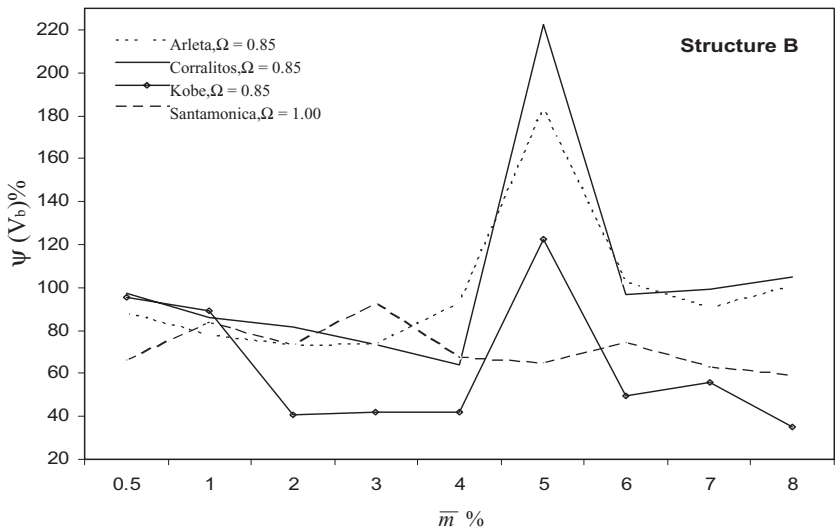

Figure 29. Variation of base shear ratio with tuned mass ratio (structure 'B')

DOI: 10.1002/tal

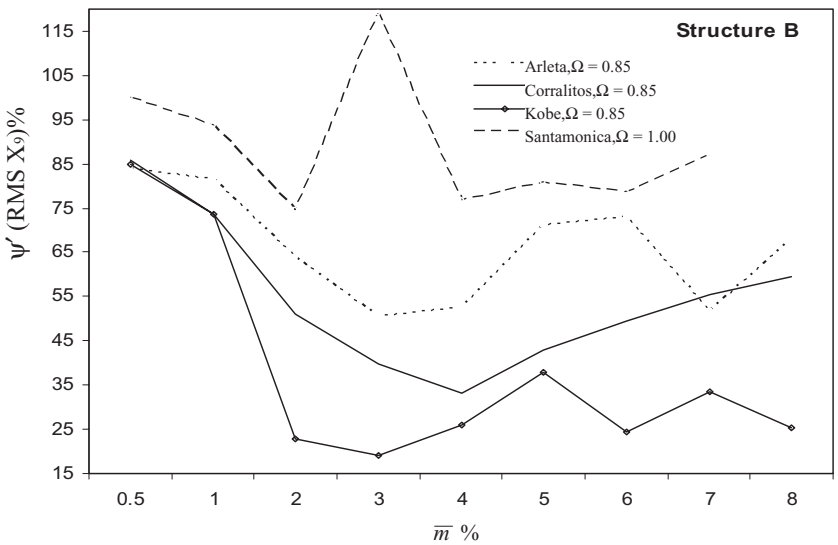

Figure 30. Variation of roof RMS displacement ratio with tuned mass ratio (structure 'B')

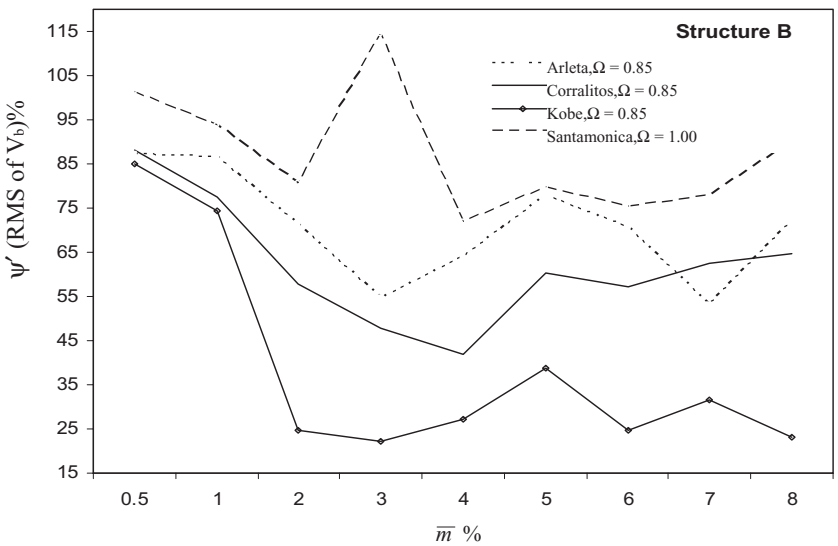

Figure 31. Variation of RMS base shear ratio with tuned mass ratio (structure 'B')

DOI: 10.1002/tal

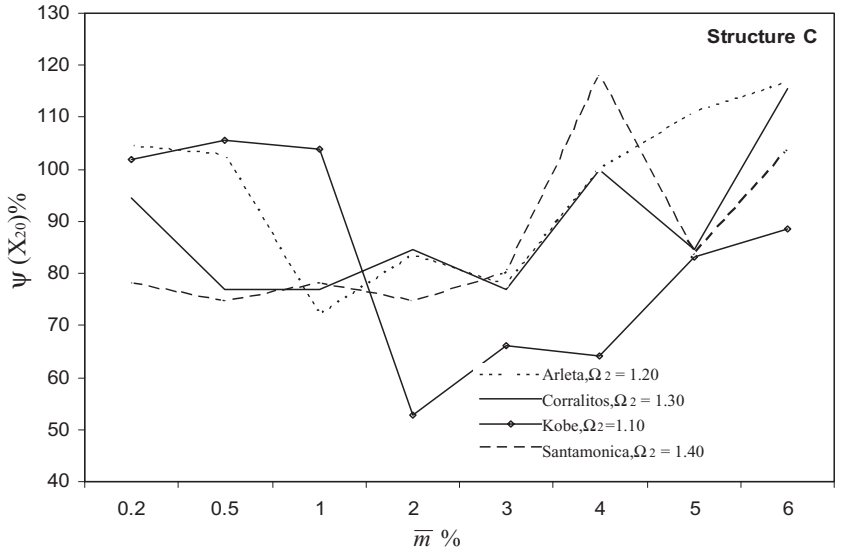

Figure 32. Variation of the 20th mass displacement ratio with tuned mass ratio (structure 'C')

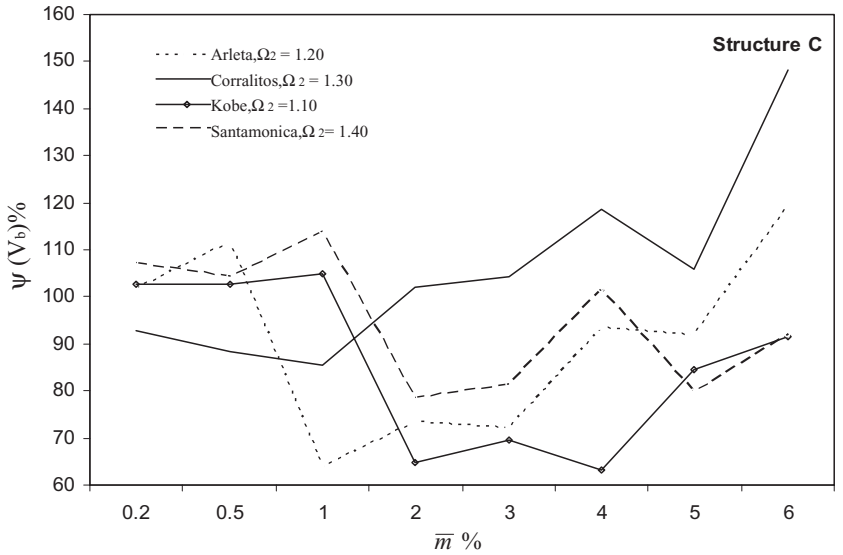

Figure 33. Variation of base shear ratio with tuned mass ratio (structure 'C')

DOI: 10.1002/tal

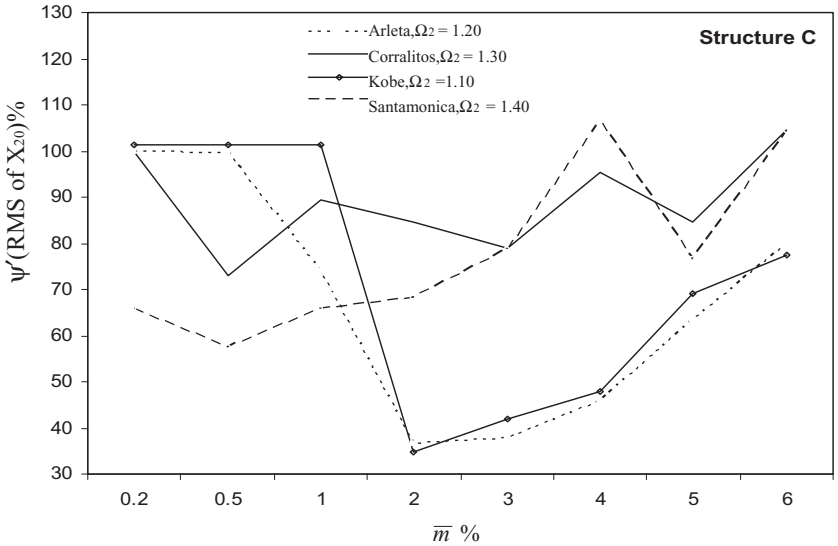

Figure 34. Variation of RMS of the 20th mass displacement ratio with tuned mass ratio (structure 'C')

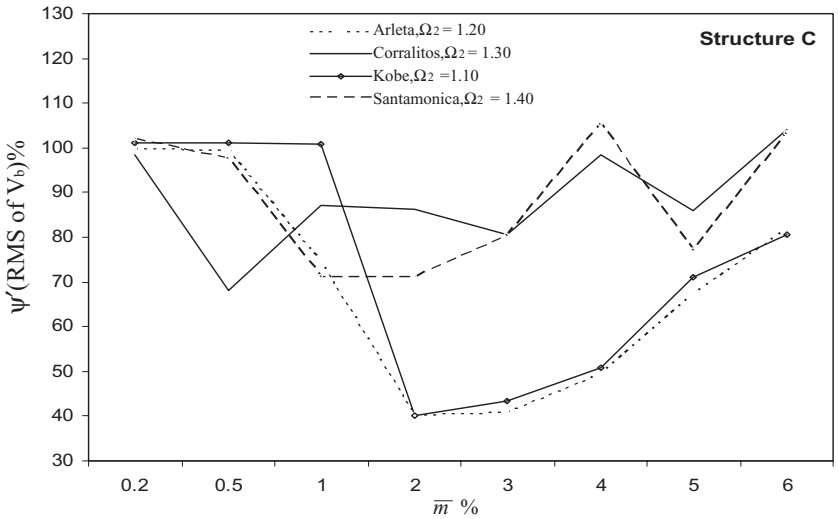

Figure 35. Variation of RMS of the base shear ratio with tuned mass ratio (structure 'C')

DOI: 10.1002/tal

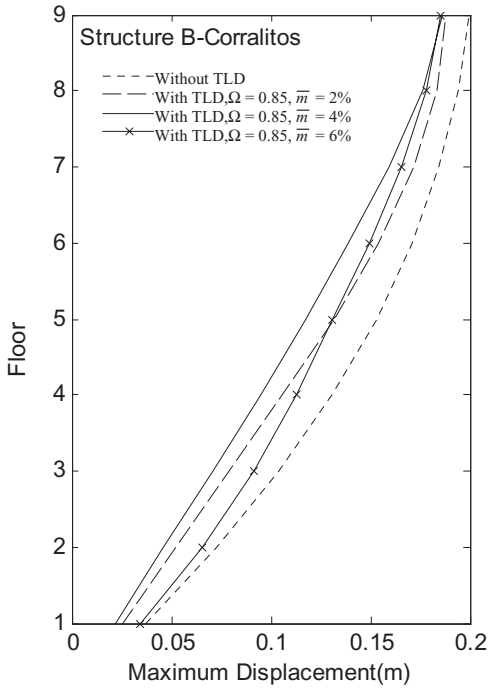

a) Corralitos

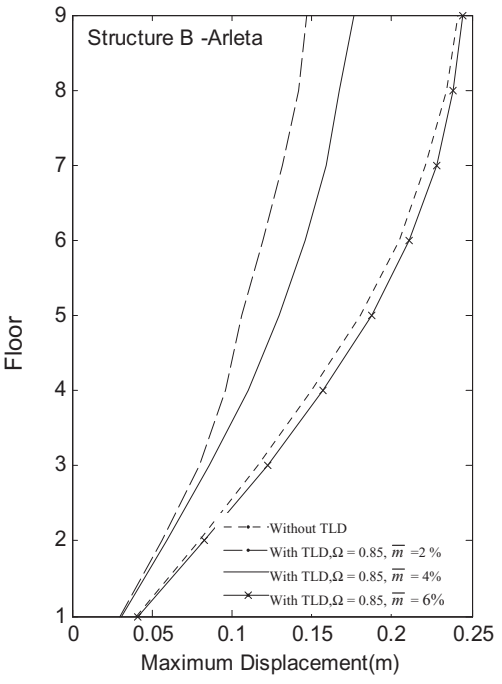

b) Arleta

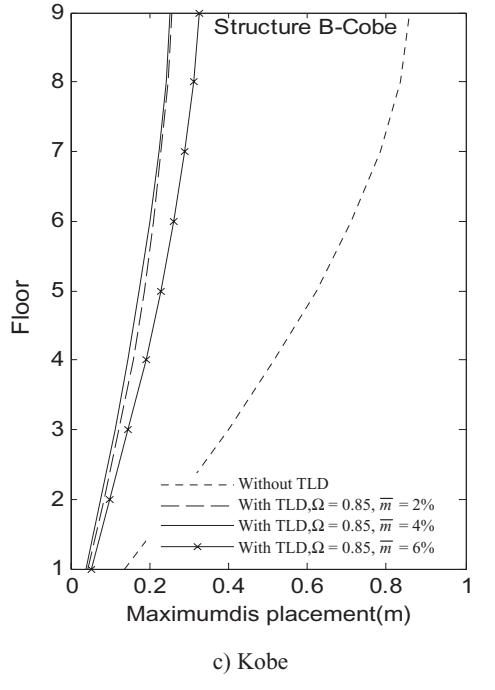

c) Kobe

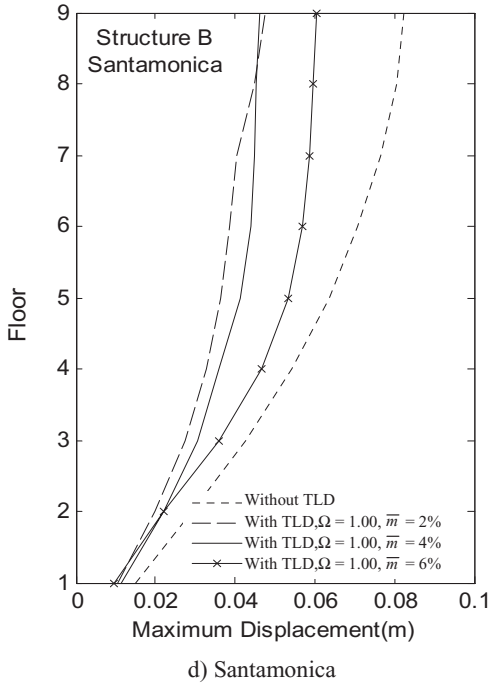

d) Santamonica

Figure 36. Variation of maximum floor displacements for different tuned mass ratios (structure 'B'): (a) Corralitos, (b) Arleta, (c) Kobe and (d) Santamonica

DOI: 10.1002/tal

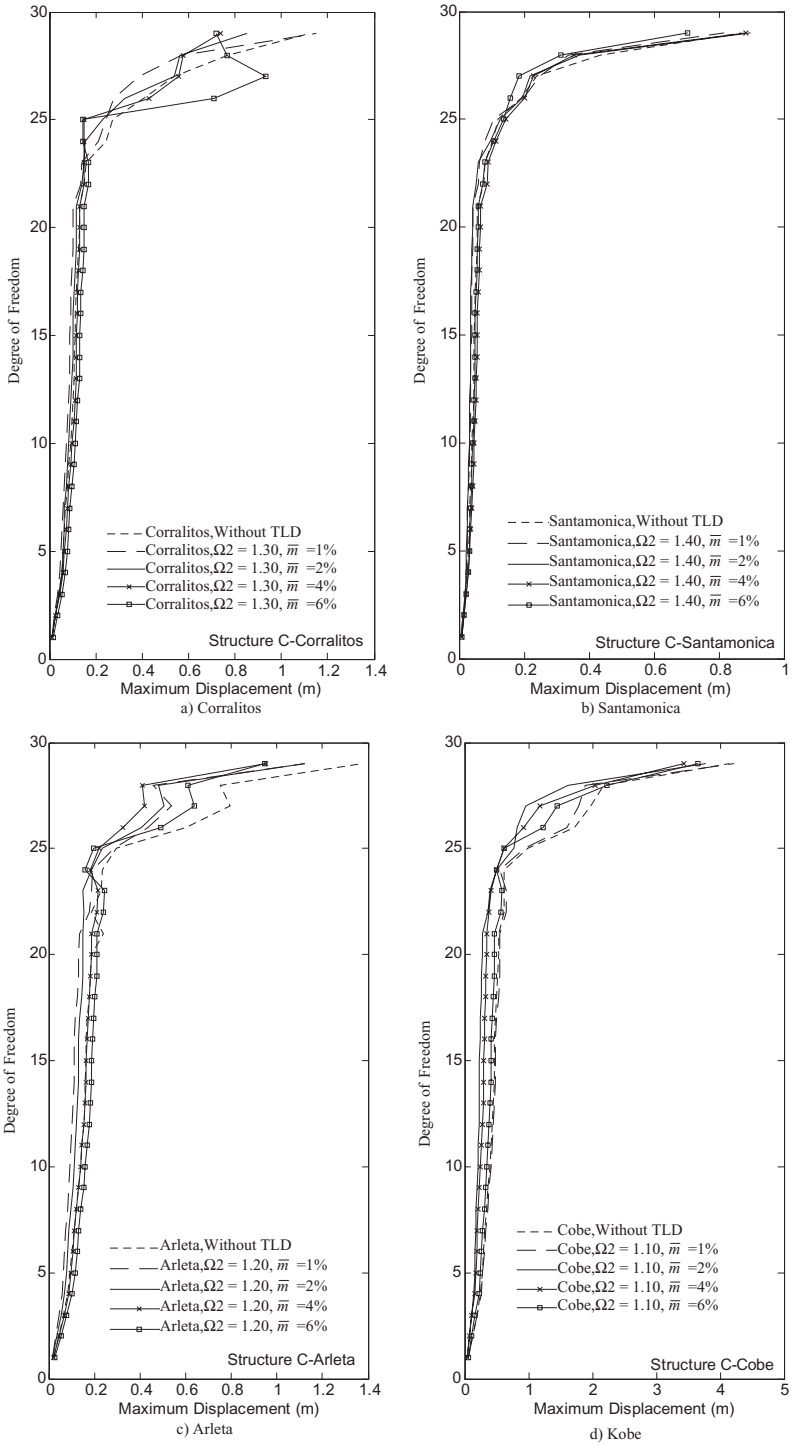

Figure 37. Variation of maximum floor displacements for different tuned mass ratios (structure 'C'): (a) Corralitos, (b) Santamonica, (c) Arleta and (d) Kobe

DOI: 10.1002/tal

formulation for three practical example systems conducting a set of parametric studies showed that the excitation amplitude and the tuning ratio are among significant factors affecting the efficiency and robustness of the TLD. The efficiency of the TLD is also found to vary with TLD mass ratio. The results suggested that the optimum mass ratio could be between 2 and 5%, and is independent of the ground motion. Using the optimum parameters described in this paper, the results of the analyses performed showed in displacement and base shear responses reductions up to 35%.

REFERENCES

Balendra T, Wang CM, Cheong HF. 1995. Effectiveness of tuned liquid column dampers for vibration control of towers. *Engineering Structures* **17**(9): 668–675.

Foss KA. 1958. Coordinates which uncouple the equations of motion of damped linear dynamic systems. *Journal of Applied Mechanics* **25**: 361–364.

Haroun MA, Pires JA, Won AYJ. 1994. Hybrid liquid column dampers for suppression of environmentally-induced vibrations in tall buildings. In *Proceedings of 3rd Conference on Tall Buildings in Seismic Regions*, Los Angeles, CA, August, 3–5.

Kaneko S, Ishikawa M. 1999. Modeling of tuned liquid damper with submerged nets. *Journal of Pressure Vessel Technology* **121**: 334–343.

Li HN, Jia Y, Wang SY. 2004. Theoretical and experimental studies on reduction of multi-modal seismic response of high-rise structures by tuned liquid dampers. *Journal of Vibration and Control* **10**: 1041–1056.

Noji, T. 1990. Study of water sloshing vibration control damper. *Journal of Structural Construction Engineering*, **411**(5): 97–105.

Noji T, Yoshida H, Tatsumi E, Kosaka H, Hagiuda H. 1988. Study on vibration control damper utilizing sloshing of water. *Journal of Wind Engineering* **37**: 557–566.

Sadek F, Mohraz B. 1998. Single and multiple tuned liquid column dampers for seismic applications. *Earthquake Engineering & Structural Dynamics* **27**: 439–463.

Sakai F, Takaeda S, Tamaki T. 1991. Tuned liquid column dampers (TLCD) for cable-stayed bridges. In *Proceedings of Specialty Conference on Innovation in Cable-stayed Bridges*, Fukuoka, Japan; 197–205.

Sun K. 1994. Earthquake responses of buildings with liquid column dampers. In *Proceedings of 5th U.S. National Conference on Earthquake Engineering*, Chicago, IL, Vol 2, 1994; 411–420.

Tait MJ, Isyumov N, El Damatty AA. 2004. The efficiency and robustness of a uni-directional tuned liquid damper and modeling with an equivalent TMD. *Wind and Structures* **7**(4): 235–250.

Veletsos AS, Ventura CE. 1986. *Modal Analysis of Non-classical Damped Linear Systems*. John Wiley & Sons: **14**: 217–243.

Wakahara T, Ohyama T, Fujii K. 1992. Suppression of wind-induced vibration of a tall building using tuned liquid damper. *Journal of Wind Engineering* **41–44**: 1895–1906.

Won AYJ, Pires JA, Haroun MA. 1996. Stochastic seismic evaluation of tuned liquid column dampers. *Earthquake Engineering & Structural Dynamics* **25**: 1259–1274.

Xu YL, Samali B, Kwok KCS. 1992. Control of along wind response of structures by mass and liquid dampers. *Journal of Engineering Mechanics (ASCE)* **118**(1): 20–39.

Yalla SK, Kareem A. 2000. Optimum absorber parameters for tuned liquid column dampers. *Journal of Structural Engineering (ASCE) 2000* **126**(8): 906–915.

Young-Kyu Ju. 2004. Structural behaviour of water sloshing damper with embossments subject to random excitation. *Can. J. Civ. Eng.* **31**: 120–132.

Yu JK, Wakahara T, Reed DA. 1999. A non-linear numerical model of the tuned liquid damper. *Earthquake Engineering & Structural Dynamics* **28**: 671–686.

DOI: 10.1002/tal